Compound Parabolic Concentrator for Pentagon Shape Absorber

Bennett Widyolar[1,2], Lun Jiang[1,2], Ali Hassanzadeh[1,2], and Roland Winston[1,2]

[1] University of California, Merced (USA)

[2] Advanced Solar Research Institute (UC Solar), Merced (USA)

Abstract

The design and development of new medium-temperature solar thermal external compound parabolic concentrator (XCPC) is presented. A nonimaging reflector is paired with an evacuated tube absorber for efficient heat collection between 100-300 °C. Several absorber geometries are simulated, with the final selection of a modified pentagon absorber shape chosen for manufacturability. The modified absorber shape, gap loss, and truncated reflector result in a geometric efficiency of 93% compared to an ideal CPC. Several selective coatings are compared for down-selection, and a Mylar reflective film with ~89% reflectance is chosen for its low cost and durability. The final prototype has a 4.56 m^2 aperture. Simulations predict an optical efficiency of 71% and thermal efficiency of 50% at 200 °C and experimental test results have confirmed an optical efficiency of 62% and a thermal efficiency near 50% at 200 °C. The stagnation temperature was measured at 333 °C. World-wide installations are presented.

Keywords: External compound parabolic concentrator, XCPC, medium temperature, nonimaging, solar thermal

1. Introduction

Low temperature collectors (<100 °C) for residential and commercial hot water typically take the form of flat plate or evacuated tube collectors, the latter of which dominates the market space due to its widespread adoption in China. Parabolic trough collectors (PTC) have historically been the most commonly used high temperature collectors (>300 °C) for industrial process heating (IPH) and concentrating solar power (CSP), but have shared the space with compact linear Fresnel (cLFR), dish, and recently with centralized solar tower installations. The space in between these two classes of collectors (100 °C < medium temperature < 300 °C) has historically been served by high temperature collectors at lower-than-design operating temperatures. Today there exist several newer options including stationary evacuated flat plates (Buonomano et al. 2016), compound parabolic concentrators (Duff et al. 2004, Kim et al. 2013), semi-tracking micro linear fresnel reflector systems (Sultana et al. 2015), semi-passive tracking combined systems (Li et al. 2017), and tracking miniature trough (Fernandez et al. 2010) and dish (Cohen and Grossman 2016) systems. The best performance of these systems typically approaches 50% conversion efficiency at 200 °C under global irradiance.

In this paper we report on the most recent round of developments to the XCPC collector, a non-tracking solar thermal collector, and the experimental performance results of the prototype tested at the University of California, Merced (UCM).

2. Collector Design

The external compound parabolic concentrator (XCPC) consists of an evacuated tube receiver paired with a nonimaging reflector and is depicted in Figure 1. Inside the evacuated tube is a selectively coated metal fin which acts as the absorbing surface of the collector. The nonimaging reflector concentrates incoming radiation over a wide range of angles onto the absorber surface. This eliminates the need for any mechanical tracking mechanism as the optics provide passive sun-tracking. The combination of concentration and an evacuated receiver allows the XCPC to reach temperatures between 100 - 300 °C.

doi:10.18086/swc.2017.31.18 Available at http://proceedings.ises.org

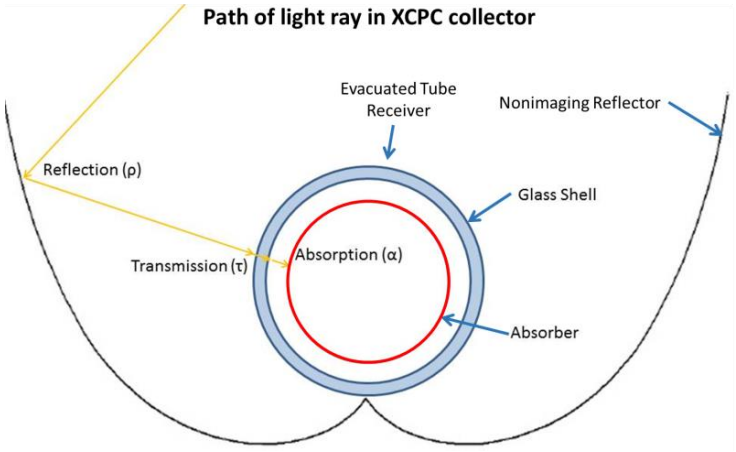

Figure 1 – Path of light ray in an XCPC collector.

The CPC profile was designed for a cylindrical absorber, but due to manufacturing limitations (specifically the geometric requirements of the ultrasonic welding machine at the prototyping facility) a new absorber geometry needed to be found. Optical simulations were performed in LightTools for the reflector profile with different absorber shapes shown in Figure 2 to determine the geometric efficiency of each case. The results of these simulations are summarized in Table 1.

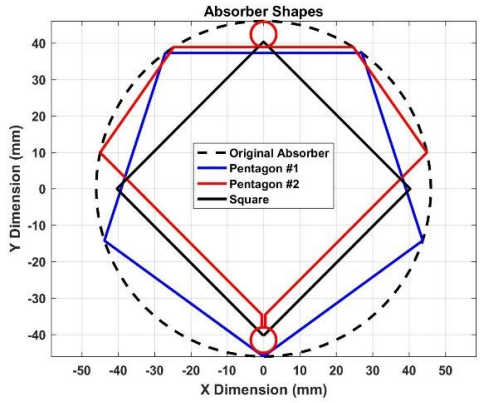

Figure 2 – Simulated absorber geometries: original circular absorber (dashed black), pentagon #1 (blue), pentagon #2 (red), and rotated square (black).

Table 1 – Geometric efficiency of CPC with different absorber shapes

Shape	Geometric Efficiency
Original Circle	1.00
Pentagon #1	0.97
Pentagon #2	0.94
Upper Tube Exposed	0.90
Lower Tube Exposed	0.84
Square	0.89

Pentagon #2 was selected after the geometry of Pentagon #1 prevented it from being welded shut by the ultrasonic welding machine. As is customary for practical reasons, the reflector was truncated to 95% of the original aperture width yielding a final design concentration ratio of 1.4X. Encasing the absorber in a glass tube results in a gap between the bottom of the absorber and the tip of the reflector. This should be minimized to reduce associated optical losses. For this design the gap was reduced to 3 mm to allow a 0.8 mm space between the absorber and the glass.

The incidence angle modifier (IAM) profile shown in Figure 4 was generated for the collector (truncated, with gap loss, and new absorber shape) by sweeping the incoming incidence angle from 0-60°.

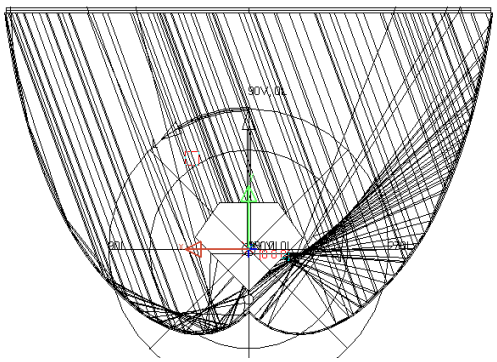

Figure 3 – Ray Trace Analysis of 40° E/W Collector with pentagon shaped absorber

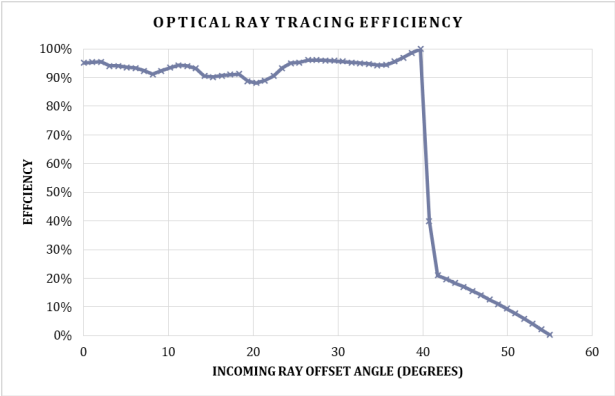

Figure 4 – Incidence Angle Modifier for 40° E/W Collector

The energy-weighted geometric efficiency η_g is calculated from Equation 1, where $\eta_{g,\theta}$ is the geometric efficiency as a function of incidence angle reported in Figure 5.

$$\eta_g = \frac{\int_0^\theta \eta_{g,\theta} \cos\theta d\theta}{\int_0^\theta \cos\theta d\theta} \qquad \text{(Eq. 1)}$$

As a result of the modified absorber shape and the 3 mm gap between the absorber and the bottom of the CPC, the total geometric efficiency is reduced to 93% compared to an ideal CPC. The optical design parameters of the final down-selected CPC design are listed in Table 2.

Table 2 – E/W XCPC Optical Design Parameters

Parameter	Value
Configuration	East-West
Acceptance Angle θ	±40°
Truncation Ratio (% of width)	0.95
Final Aperture Width	406 mm
Absorber Shape	Pentagon
Absorber Perimeter	285 mm
Concentration Ratio	1.4X

3. Materials Selection and Prototype Development

A selective coating is designed to absorb as much of the solar spectrum as possible while emitting as little as possible during operation. Several commercial flat-absorber vacuum tubes with different coatings were placed side by side outdoors, with thermocouples inserted to measure temperature. They were all uncovered at the same time and the temperature rise was recorded. The results showed a difference in performance between suppliers. Most coatings exhibited performance differences between batches, however, the Sunselect and TiNoX coatings showed stable quality and performance and were down-selected for a second round of testing. The second round of testing was performed again with the two commercially available flat absorber vacuum tubes, and for two coating manufacturers who were able to supply material for the prototype XCPC absorber. An image of the test setup is shown in Figure 5 and the results of the second test are presented in Figure 6.

As a result of these tests, SunSelect applied over a copper substrate was down-selected as the selective coating for the E/W XCPC prototype. The coating has a solar-weighted absorptance of 95% and an emissivity of 5% at 100 °C.

Borosilicate glass is typically used in solar applications because of its high solar transmittance. A borosilicate glass sample from the glass tube supplier was tested at NREL in 2007 and the transmission profile is presented in Figure 7. A total solar-weighted transmission of 91.7% is obtained which is consistent with the two Fresnel losses

going in and out of the glass.

Figure 5 – Side-By-Side Stagnation Test Setup

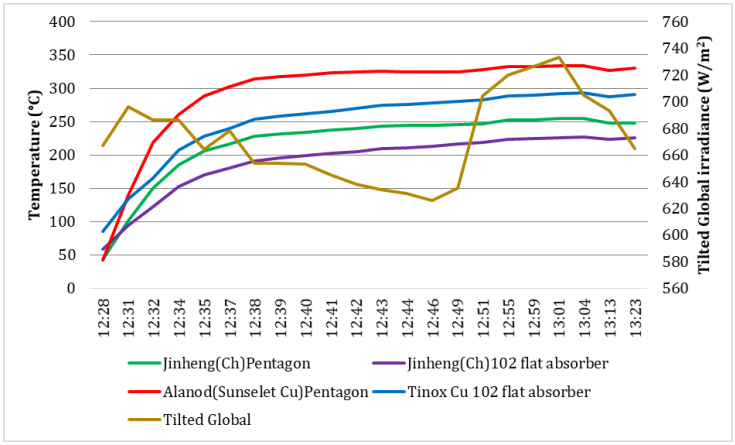

Figure 6 - Stagnation test results.

Several commercial reflector materials exist with high reflectance (>90%) and good outdoor stability. At the time of prototyping a reflective Mylar film was found for roughly $1/m^2. The hemispherical reflectance of the film was measured at 89%, which was maintained after 2 years of outdoor exposure (see Figure 8). As a result the film was selected for the E/W XCPC prototype reflector.

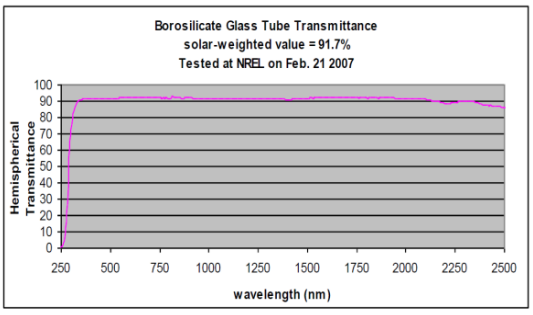

Figure 7 – Borosilicate glass transmission profile tested at NREL in 2007. The solar-weighted transmission is 91.7%.

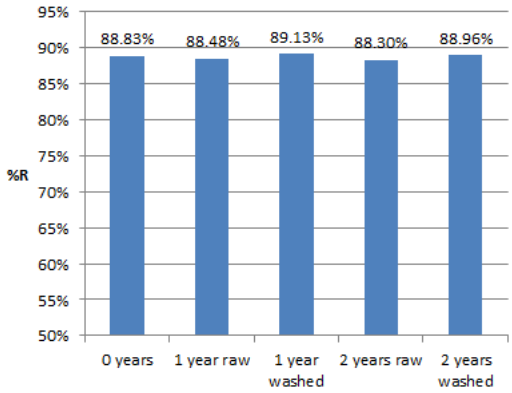

Figure 8 – Aluminized polymer film reflectance over time

A rendering of the final prototype design is shown in Figure 9 with a close up of the plumbing connections in Figure 10. Final specifications for the prototype are listed in Table 3.

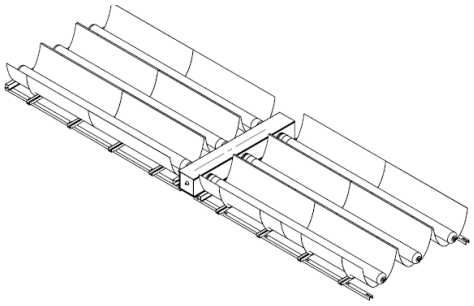

Figure 9 – Final E/W XCPC collector prototype. 6 CPCs are plumbed off a centralized manifold box.

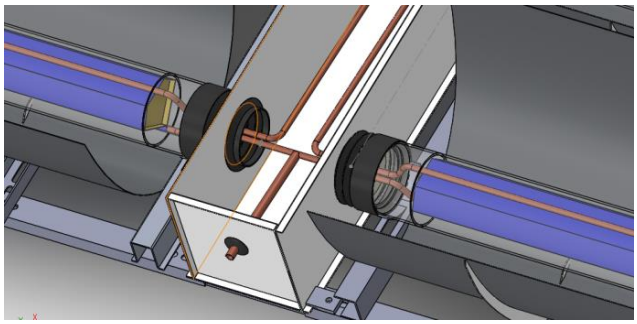

Figure 10 – Manifold Connections – Each side of the collector has 3 CPCs plumbed in series and both sides are plumbed in parallel.

Inside the evacuated glass tube is the selectively coated copper fin formed into the shape of a pentagon. A copper pipe is ultrasonically welded to the top and bottom of the pentagon with a 180° U-bend at the end. The copper pipe transitions into the glass tube via a glass to metal seal and the entire tube is evacuated and sealed below 10^{-4} mbar. A gas getter maintains the vacuum integrity and provides visual indication of vacuum quality.

The reflectors are formed of aluminum and overlaid with a reflective Mylar film. Their shape is supported by 4 ribs along the length of each reflector. The entire collector is formed by combining three XCPCs on either side of a central manifold box. Inside the manifold box, the tubes are piped together using copper flare connections and surrounded with fiberglass insulation. The two sides of the manifold box are piped in parallel, each with three CPCs piped in series.

Table 3 – E/W XCPC Collector Prototype Specifications

Parameter	Value
Selective Coating	SunSelect
Solar Weighted Absorptance (α)	0.95
Emissivity ($\varepsilon_{100\,°C}$)	0.05
Copper Pipe OD	8 mm
Copper Pipe Thickness	0.75 mm
Absorber Tube Length	1.9 m
Glass Material	Borosilicate
Solar Weighted Transmission (τ)	0.92
Glass Tube OD	102 mm
Glass Tube Thickness	2.2 mm
Reflector Material	Mylar
Total Hemispherical Reflectance (ρ)	0.89
CPCs per Collector	6
Aperture Area	4.5 m^2
Gross Area	5.4 m^2

4. Optical and Thermal Performance Models

Simulation of the completed design was performed in LightTools for 1 million rays using optical parameters of the materials used in the XCPC prototype. Ray trace diagrams are presented in Figure 11. At normal irradiance, an optical efficiency η_0 of 71% is obtained.

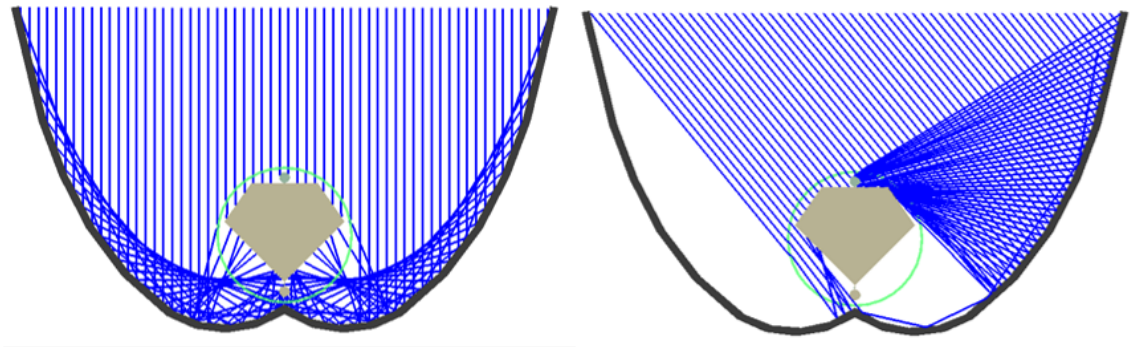

Figure 11 – Ray tracing of E/W XCPC collector for normal incidence and off-angle incidence.

A two-dimensional finite element model was created for the absorber where the polygonal fin shape was approximated by a generic 20-sided polygon (shown for n = 6 in Figure 12) and the tube length was divided into 40 nodes.

Uniform solar irradiance is assumed to be incident on all fins, which also radiate outward and conduct with their radial and axial neighbors. The fins at the top and bottom of the absorber are assumed to be at thermal equilibrium with the copper pipe, providing a conduction pathway to the interior surface of the pipe where heat is transferred to the fluid via convection. Since the absorber tubes are evacuated, no other convection is modelled. The heat

transfer coefficient between the inner pipe wall and the fluid is calculated based on the Nusselt number for laminar flow and using the Gnielinski and Dittus-Boelter correlations for turbulent flow.

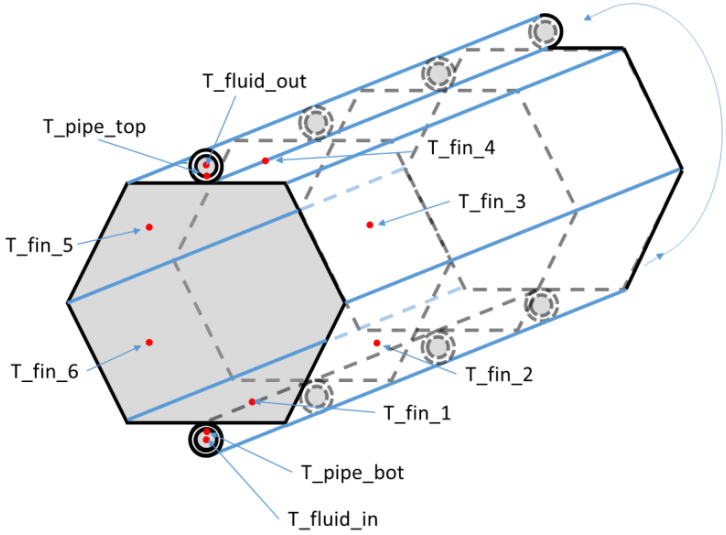

Figure 12 – Finite Element Analysis Mesh. The pentagon absorber is approximated by an n-sided polygon (shown for 6 sides here). The actual model used a 20-sided polygon and the length of the absorber was divided into 40 nodes.

Table 4 – Heat transfer model parameters

Parameter	Value
L_abs	1.8 m
n	40 nodes
L_fin	272 mm
n_fins	20 nodes
Fin_thickness	0.125 mm
Fin and Pipe material	Copper (Cu)
Piper inner diameter	6.5 mm
Pipe outer diameter	8 mm
G	1000 W/m^2
$\dot{m}$	75 g/s
k_{Cu}	400 W/m-K
ε	0.05 @ 100 °C, 0.08 assumed @ 200 °C

The parameters used in the model are listed in Table 4, assuming fluid properties for the mineral oil Duratherm 600. The emissivity of the selective coating is known to be 0.05 at 100 °C and was interpolated linearly to an emissivity of 0.08 at 200 °C. Matrix inversion was used to solve for the temperature at each node and the process was repeated until the temperature change between iterations was less than 0.01 °C.

The input solar irradiance to the model is calculated according to equation 2 and the solar irradiance absorbed by each fin from equation 3.

$$Q_{in} = A_{absorber} C_x G \qquad \text{(Eq. 2)}$$

$$Q_{fin,absorbed} = \frac{Q_{in}\eta_0}{n_{fins} n} \qquad \text{(Eq. 3)}$$

The net thermal generation of the collector ($Q_{thermal}$) is calculated based on the inlet and outlet temperatures from the model. This simulation was performed for temperatures between 25 °C to 400 °C and the efficiency calculated according to equation 5 is plotted versus temperature in Figure 13.

$$Q_{thermal} = \dot{m} c_p \Delta T_{col} \quad \text{(Eq. 4)}$$

$$\eta = \frac{Q_{thermal}}{Q_{in}} \quad \text{(Eq. 5)}$$

The efficiency jump between 125/150 °C is due to the transition from laminar to turbulent flow at which point the calculation of the heat transfer coefficient between the pipe wall and the fluid changes. Average temperatures along the length of the tube are presented in Figure 14 for an inlet temperature of 200 °C, showing a maximum temperature rise along the fin length of 40 °C.

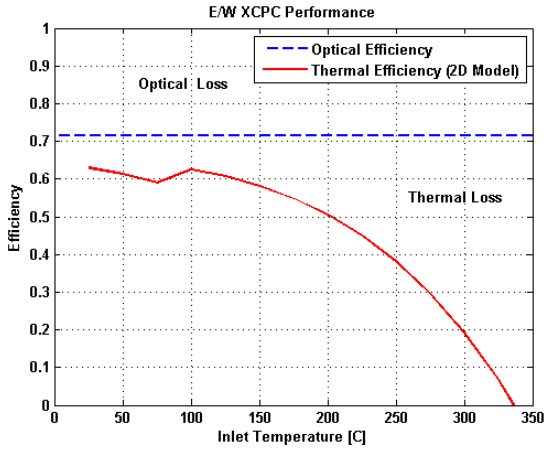

Figure 13 – Simulated performance results for an input irradiance of 1000 W/m².

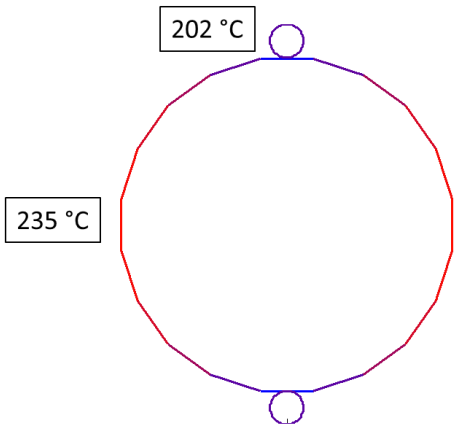

Figure 14 – Temperature profile of fins for an inlet temperature of 200 °C.

5. Experimental Test Results

Performance of the prototype XCPC collector was tested at the University of California Merced Castle Research Facility. In this section is a description of the test platform, testing methods, and experimental performance results.

The half-collector prototype (3 tubes) was mounted on a dual axis tracker to measure on and off-axis performance for characterization. A precision spectral pyranometer (PSP) and normal incidence pyrheliometer (NIP) mounted on the tracker measure the solar resource. The main test platform is a medium temperature oil loop (Figure 15) which contains a circulation pump, primary heating element, coriolis flow meter, thermocouple clusters, and an in-line calorimeter. A total of 33 sensors are installed in the system, including: 1 Coriolis flow meter (± 0.1 %); 25 K-type thermocouples, 4 pressure gauges, 1 current clamp sensor, 1 Precision Spectral Pyranometer (PSP), and 1 Normal Incidence Pyrheliometer (NIP). Data is collected using an Agilent 34970A data acquisition unit, which scans and records all sensor readings every 5 seconds. The instrument and measurement error are listed in Table 5.

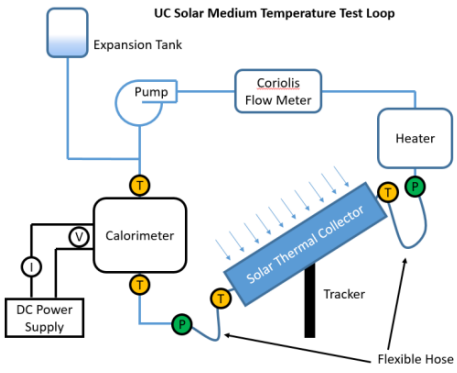

Figure 15 – UC Solar Medium Temperature Test Loop Schematic

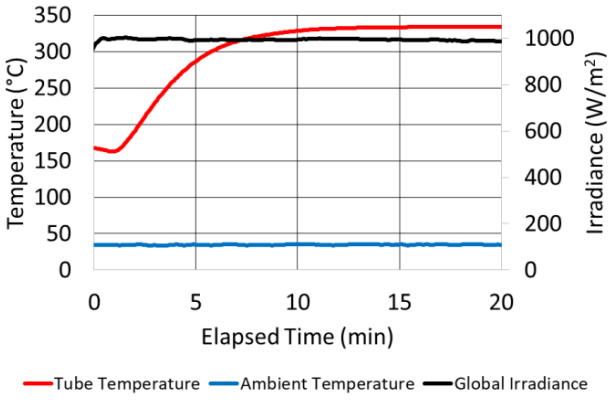

Figure 16 – Stagnation test results

Table 5 – Instrument and measurement error

Device	Instrument Error	Keysight Measurement Error	Temperature Coeff. [/°C ambient above 28°C]
k-Type thermocouple	±1.1°C or 0.4% (whichever is greater)	±1.0°C	+0.03%
Coriolis Mass Flow Meter	±0.1% of reading	±0.01% of reading	+0.001% of reading
UNI-T UT210 current clamp meter	±2.0% of reading	NA	NA
DC Voltage Measurement	NA	±0.0045% of reading + 0.003% of range	±0.0005% of reading + 0.0003% of range
Precision Spectral Pyranometer (PSP)	±2.5% of reading	±0.0050% of reading + 0.0040 of range	±0.0005% of reading + 0.0005% of range
Normal Incidence Pyrheliometer (NIP)	±2.5% of reading	±0.0050% of reading + 0.0040 of range	±0.0005% of reading + 0.0005% of range

A stagnation test was performed on August 11, 2017. Three thermocouples inserted at various lengths inside the upper fluid channel of a single evacuated tube on the XCPC collector measure the temperature over time. The results of this test are shown in Figure 16. The inside of the evacuated tube reached a final stagnation temperature of 333 °C.

Optical testing was performed between August 20th and September 6th using the setup shown in Figure 17. The efficiency is calculated according to equation 6, where $\dot{m}$ is the mass flow rate of the HTF in kg/s, c_p is the heat capacity of the fluid in kJ/kg-K, ΔT_{col} is the temperature difference across the collector in °C, A_{col} is the aperture area of the collector in m^2, and G is the global solar irradiance in kW/m^2.

$$\eta_{thermal,flow} = \frac{Q_{thermal,flowrate}}{Q_{solar}} = \frac{\dot{m}c_p\Delta T_{col}}{A_{col}G} \qquad \text{(Eqn. 6)}$$

These tests were performed using city water as the heat transfer fluid. Thermocouple clusters measured the average inlet and outlet temperature and the flow rate was measured manually by recording the time it took to fill up a 5 gallon bucket (which actually contains 5.6 gallons). The heat capacity of water was assumed to be a constant 4.18 kJ/kg-K. Results are presented in Figure 18 from which an average optical efficiency of 62% was obtained.

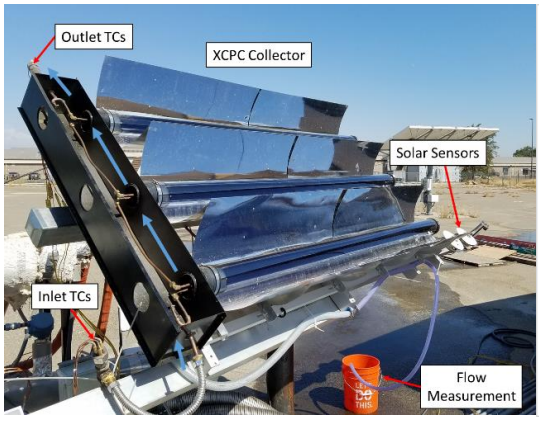

Figure 17 – Optical Testing

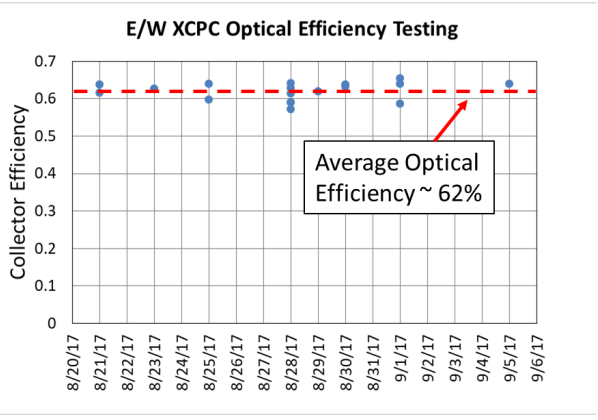

Figure 18 – Optical Test Results

The XCPC collector (Figure 19) was tested at elevated temperatures using the oil test loop. The instantaneous thermal efficiency of the collector was calculated using the standard flow rate method (equation 7) and also using

a calorimetric technique discussed below.

A calorimeter installed in-line with the solar collector generates heat using two 1 kW resistive heating elements placed inside two counter-flow tubes. The heat transfer oil enters the outer annulus of the counter-flow tube and exits through the inner annulus where it is in direct contact with the heating element (Figure 20). The two heating elements and oil flow path are constructed in parallel and the entire calorimeter is wrapped in aerogel insulation with the heated portions encased in all glass vacuum tubes to limit heat loss to the environment. Two k-type thermocouple clusters containing six thermocouples each measure the inlet and outlet temperatures of the calorimeter.

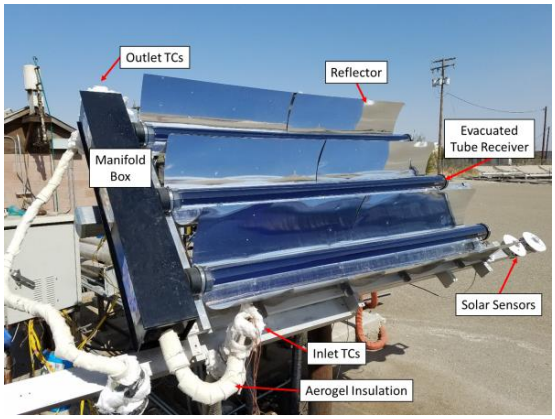

Figure 19 – Oil Testing

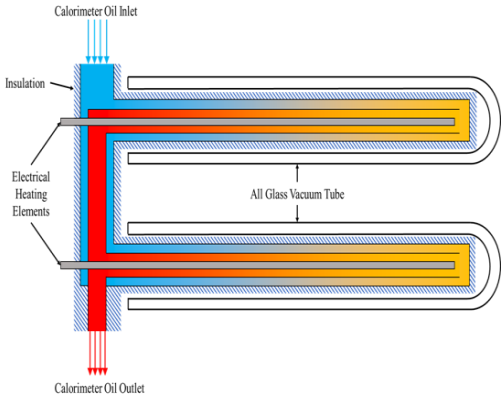

Figure 20 – Calorimeter Schematic

Since the calorimeter is plumbed in-line with the collector it sees the same heat transfer fluid (C_p) and flow rate as the collector. A known amount of power input generates a repeatable temperature rise across the calorimeter. By comparing the temperature rise across the calorimeter to the temperature rise across the collector, the power output of the collector can be determined. For example if the collector raises the temperature 10 °C and the calorimeter also raises the temperature 10 °C from 2 kW of power, we know the collector is generating 2 kW of thermal power.

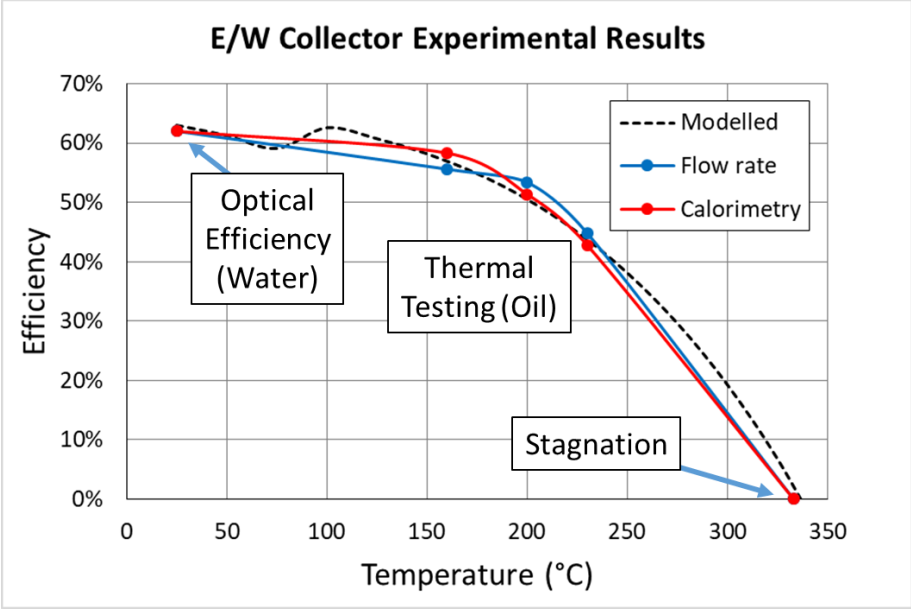

Figure 21 – Experimental Results

The use of a calorimeter provides a redundant measurement which eliminates the flow rate measurement and dependence on heat capacity which is prone to change from the manufacturers specifications over time. Instead they are replaced by more reliable temperature, current, and voltage measurements. The thermal efficiency

determined by the calorimeter is calculated according to equation 7, where ΔT_{cal} is the temperature rise across the calorimeter, V_{cal} is the DC supply voltage, and I_{cal} is the DC current. Results are presented in Figure 21.

$$\eta_{thermal,cal} = \frac{\mathrm{Q_{thermal,cal}}}{\mathrm{Q_{solar}}} = \frac{\frac{\Delta T_{col}}{\Delta T_{cal}} \cdot V_{cal} \cdot I_{cal}}{A_{col} G} \qquad \text{(Eq. 7)}$$

6. Installations

Figure 22 – Merced, CA Installation

The Merced installation shown in Figure 22 is a 20 kW array of the E/W collectors described in this paper installed alongside an earlier generation 20 kW N/S array. These arrays are used to provide thermal power for various projects including solar cooling (Widyolar et al. 2014), solar drum drying (Ferry et al. 2016), and is currently being commissioned for solar wastewater evaporation.

Some representative data is presented below in Figures A, and B for September 8th, 2016. The total solar energy incident on plane of the collector array between 11:45 pm and 5:00 pm was 175.5 kWh, resulting in a thermal generation of 76.9 kWh and 70.6 kWh of cooling from the chiller.

Experimental testing on a single E/W collector showed an efficiency of 55% at an operating temperature of 160 °C while the efficiency of the array tested in this experiment at the same temperature was around 44%. The decrease is attributed to heat losses through the insulated pipes which interconnect the collectors in the array. A rough calculation shows this is on the order of 2-3 kW from the 150 m of ¾" pipe insulated with 2" of fiberglass. Accounting for this heat loss makes the data from this experiment consistent with the previously reported test results. The E/W array took approximately 2 hours to warm up to an outlet temperature of 180 °C and provided 15-20 kW of direct solar powered cooling for an additional 6 hours. A solar COP of 0.44 demonstrated by the E/W array is comparable with other documented double effect solar thermal cooling systems.

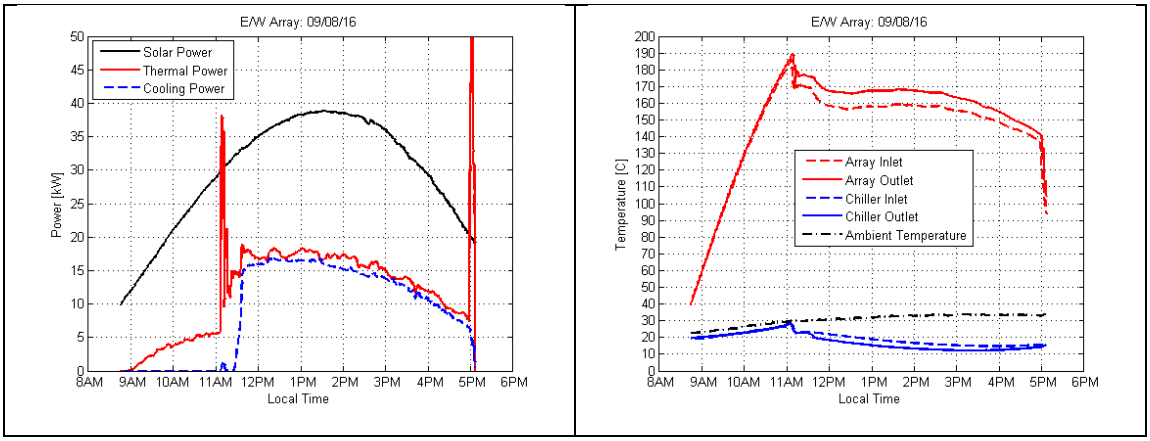

Figure 23 – Sept 8th, 2016 – E/W Array Performance	Figure 24 – Sept 8th, 2016 – E/W Array Temperatures

Table 7 – East-West Array – September 8th, 2016

		Range (instantaneous)	Operational Average*
Collector efficiency	Thermal power captured at 160 °C per available solar power.	0.350 – 0.565	0.438
Thermal COP	Cooling power per captured thermal power	0.721 – 1.101	0.919
Solar COP	Cooling power per available solar power	0.288 – 0.488	0.402

*Operational average taken between 11:45 am and 5:00 pm.

Figure 25 – UlaanBaatar, Mongolia Installation

The Mongolia installation shown in Figure 25 is a 5 kW E/W array installed to provide space heating (Winston et al. 2014). The collector system is installed completely off-grid, using a small PV panel to power a 24 VDC circulation pump which circulates antifreeze through the collector array. The heat is transferred into the ger by a heat exchanger, which is stored in 55 gallon insulated drums of hot water.

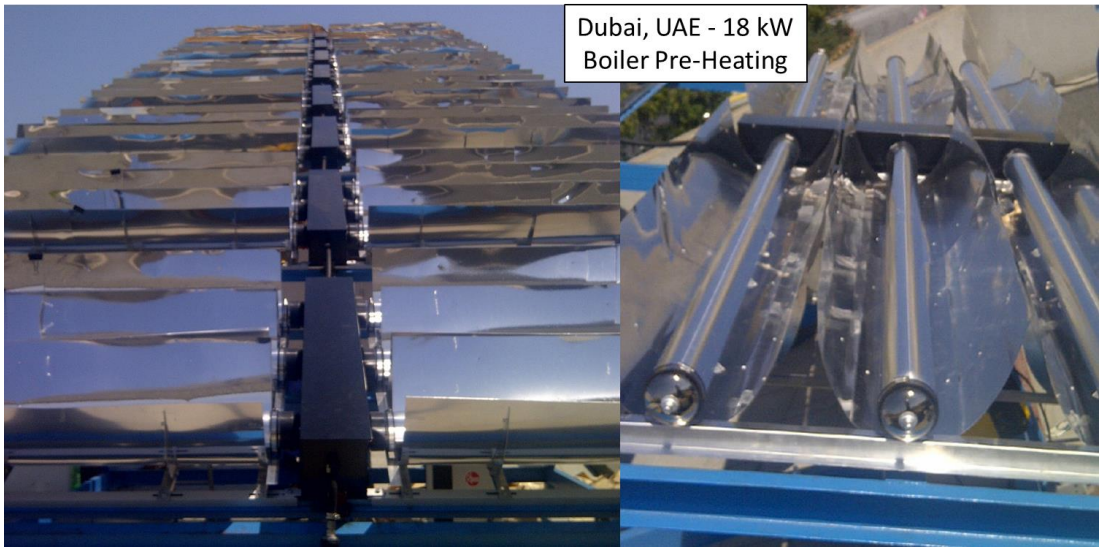

Figure 26 – Dubai, UA Installation

The Dubai installation shown in Figure 26 is the most recent installation and is currently being used to provide boiler pre-heating for sugar refining.

7. Conclusion

In this paper we present the most recent round of developments on the external compound parabolic concentrator (XCPC). The XCPC is a wide-angle concentrator which allows it to (1) collect sunlight year-round from a stationary position, (2) accommodate installation misalignment, and (3) collect a significant fraction of the diffuse solar resource while still providing 1.4X concentration on the absorber. The evacuated tube absorber allows efficient operation regardless of external climate conditions (hot or cold). Optical and thermal simulations have match the experimental data very closely. The collector has an optical efficiency of 62% and a thermal efficiency of 59% at 100 °C and 50% at 200 °C. Current installations are located in California, Mongolia, and the United Arab Emirates and the technology is being commercialized in the USA and India.

8. References

Buonomano, A., Calise, F., d'Accadia, M.D., Ferruzzi, G., Frascogna, S., Palombo, A., Russo, R. and Scarpellino, M., 2016. Experimental analysis and dynamic simulation of a novel high-temperature solar cooling system. Energy Conversion and Management, 109, pp.19-39.

Cohen, S., Grossman, G., 2016. Development of a solar collector with a stationary spherical reflector/tracking absorber for industrial process heat. Solar Energy. 128, 31-40.

Duff, W., Winston, R., O'Gallagher, J., and Bergquam, J., 2004. Performance of the Sacramento demonstration ICPC collector and double effect chiller. Solar Energy. 76, 175-180.

Fernández-García, A., Zarza, E., Valenzuela, L., Pérez, M., 2010. Parabolic-trough solar collectors and their applications. Renewable and Sustainable Energy Reviews. 14, 1695-1721.

Ferry, J., Alleyne, F., Milczarek, R., Winston, R. and Olson, D., 2016. Efficiency and Design Analysis of a Solar Thermal Powered Flat Plate Dryer. In ASABE Annual International Meeting (p. 1). American Society of Agricultural and Biological Engineers.

Kim, YS., Balkoski, K., Jiang, L. and Winston, R., 2013. Efficient stationary solar thermal collector systems operating at a medium-temperature range. Applied Energy. 111, 1071-1079.

Li, Q., Zheng, C., Shirazi, A., Mousa, O., Moscia, F., Scott, J., 2017 Design and analysis of a medium-temperature, concentrated solar thermal collector for air-conditioning applications. Applied Energy. 190, 1159-1173.

Sultana, T., Morrison, G., Taylor, R., Rosengarten, G., 2015. TRNSYS modeling of a linear fresnel concentrating collector for solar cooling and hot water applications. Journal of Solar Energy Engineering. 137.

Widyolar, B., Winston, R., Jiang, L. and Poiry, H., 2014. Performance of the Merced Demonstration XCPC Collector and Double Effect Chiller. Journal of Solar Energy Engineering, 136.

Winston, R., Widyolar, B. and Jiang, L., 2014. Nonimaging Optics Heating up Mongolia's Harsh Winter. In SPIE Optical Engineering+ Applications (pp. 91910D-91910D). International Society for Optics and Photonics.